Preparation and Structure of $[AsPh_4]_2[HFe_7(CO)_{20}B]$. Evidence for the Sequential Encapsulation of a Boron Atom into an Iron Cage by a Radical-Driven Cluster-Building Process

Ananda Bandyopadhyay, Maoyu Shang, Chang Soo Jun, and Thomas P. Fehlner*

Department of Chemistry and Biochemistry, University of Notre Dame, Notre Dame, Indiana 46556

Received April 6, 1994®

The sequential formation of $[HFe_5(CO)_{15}B]^{2-}$ (**1**), $[HFe_6(CO)_{17}B]^{2-}$ (**2**), and $[HFe_7(CO)_{20}B]^{2-}$ (**3**) in the facile reaction of $[Fe_4(CO)_{12}HB]^{2-}$ with either $Fe_2(CO)_9$ or $Fe(CO)_3(cco)_2$ (cco = *cis*-cyclooctene) is demonstrated. Complexes **1** and **2** were characterized spectroscopically as partially opened boride clusters whereas spectroscopic and X-ray crystallographic analyses ($AsPh_4$ salt; monoclinic, $P2_1/c$; a = 11.248(2) Å, b = 14.336(2) Å, c = 41.698(6) Å, β = 90.30(1)°, V = 6724(2) Å^3, Z = 4; R_1 = 0.042, R_2 = 0.057) of **3** show it to be a closed boride. The boron atom resides inside a trigonal prismatic array of six iron atoms, with the seventh capping one of the rectangular faces. The characteristics of the reaction suggest a cluster-building process initiated by electron transfer from $[Fe_4(CO)_{12}HB]^{2-}$ to $Fe_2(CO)_9$ leading to a radical-anion-mediated cluster-building process in which $Fe(CO)_5$ is the byproduct.

Introduction

Transition metal clusters containing interstitial atoms constitute a substantial subsection of the chemistry of discrete as well as extended cluster systems.[1,2] The most fully discussed centered clusters are those containing group 14 and higher elements.[3] These clusters exhibit a range of structures with varying numbers of metal atoms. Several routes to clusters with interstitial atoms are known and a few have been illucidated in some detail. Generally speaking, however, mechanistic information on cluster reactions is sparse[1] and the situation is no different with clusters containing interstitial atoms.

Compounds containing hydrogen and other lighter elements as interstitial atoms have also been described.[4] However, the driving force for the incorporation of an electron-rich atom like phosphorus into a cluster is almost certainly different from that of an orbital-rich atom like boron. Thus, the latter presents both a synthetic challenge and a significantly interesting variation of an important metal cluster theme.

Since an early report of a possible boride cluster,[5] three groups have addressed the synthesis of cluster borides in a systematic manner. Housecroft et al. have used the replacement of H with $AuPR_3$ to form borides with gold atoms forming part of the metal shell (Chart 1a).[6] In another approach they have reacted $[Ru_3(CO)_9B_2H_5]^-$ with $Ru_3(CO)_{10}(NCMe)_2$ to give a trigonal prismatic boride, i.e., Chart 1b,[7] and recently reported degradation of this cluster into a five ruthenium atom boride characterized as a gold derivative.[8] Shore et al. have synthesized a ruthenium boride from $Ru_3(CO)_{12}$ and BH_3·L (Chart 1c),[9] and the same compound, albeit with a differing arrangement of CO ligands,

Chart 1

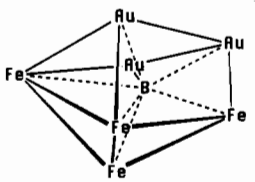

a. $Fe_4(CO)_{12}Au_3(PPh_3)_3B$

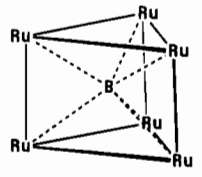

b. $[H_2Ru_6(CO)_{18}B]^-$

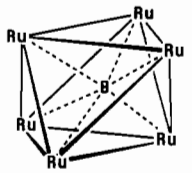

c. $HRu_6(CO)_{17}B$

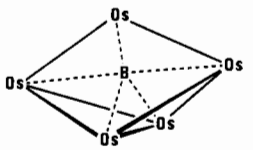

d. $HOs_5(CO)_{16}B$

has also been reported by Housecroft et al.[10] Shore has also utilized the $H_3Os_3(CO)_9BCO$ cluster as the thermal precursor of a five osmium atom boride (Chart 1d) as well as closely related compounds.[11] Our work, contemporary with that described, has been focused on the analogous iron systems, and as it constitutes the origin of the present study, a brief summary follows.

Figure 1 summarizes the pertinent older results. Our first contribution was the demonstration of the clean, quantitative cluster building reaction (1).[12] Later we showed that

$$[HFe_3(CO)_9H_2BH]^- + 2Fe_2(CO)_9 \rightarrow [HFe_4(CO)_{12}HB]^- + H_2 + 3Fe(CO)_5 \quad (1)$$

$[HFe_3(CO)_9H_2BH]^-$ itself can be made in good yield by the direct reaction of BH_3·L with iron carbonyl compounds that produce $Fe(CO)_x$ fragments under mild conditions, i.e., $Fe_2(CO)_9$[13] and $Fe(CO)_3(cco)_2$ (cco

* Abstract published in *Advance ACS Abstracts,* August 1, 1994.

(1) *The Chemistry of Metal Cluster Complexes*; Shriver, D. F., Kaesz, H. D., Adams, R. D., Ed.; VCH: New York, 1990.
(2) Corbett, J. D. *Chem. Rev.* **1985**, *85*, 383.
(3) Gonzalez-Moraga, G. *Cluster Chemistry. Introduction to Transition Metal and Main Group Element Clusters*; Springer-Verlag: New York, 1993.
(4) Housecroft, C. E. In *Inorganometallic Chemistry*; Fehlner, T. P., Ed.; Plenum Press: New York, 1992; p 73.
(5) Schmid, G.; Bätzel, V.; Etzrodt, G.; Pfeil, R. *J. Organomet. Chem.* **1975**, *86*, 257.
(6) Harpp, K. S.; Housecroft, C. E.; Rheingold, A. L.; Shongwe, M. S. *J. Chem. Soc., Chem. Commun.* **1988**, 965.
(7) Housecroft, C. E.; Matthews, D. M.; Rheingold, A. L.; Song, X. *J. Chem. Soc., Chem. Commun.* **1992**, 842.
(8) Housecroft, C. E.; Matthews, D. M.; Rheingold, A. L. *Organometallics* **1992**, *11*, 2959.
(9) Hong, F. E.; Coffy, T. J.; McCarthy, D. A.; Shore, S. G. *Inorg. Chem.* **1989**, *28*, 3284.
(10) Draper, S. M.; Housecroft, C. E.; Keep, A. K.; Matthews, D. M.; Song, X.; Rheingold, A. L. *Organomet. Chem.* **1992**, *423*, 241.
(11) Chung, J.-H.; Knoeppel, D.; McCarthy, D.; Columbie, A.; Shore, S. G. *Inorg. Chem.* **1993**, *32*, 3391.
(12) Housecroft, C. E.; Fehlner, T. P. *Organometallics* **1986**, *5*, 379.
(13) Meng, X.; Fehlner, T. P. *Inorg. Synth.* **1992**, *29*, 269.

0020-1669/94/1333-3677$04.50/0

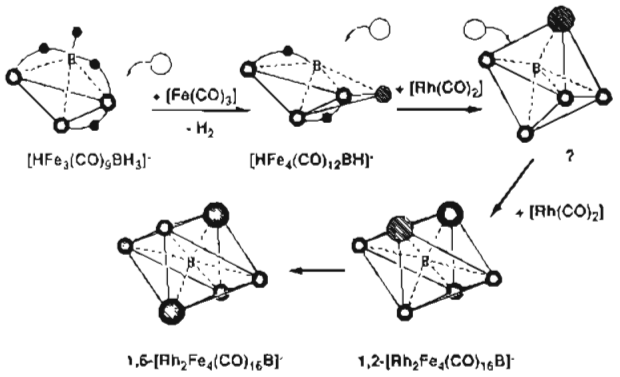

Figure 1. Schematic drawing of known high-yield cluster-building reactions. $Fe_2(CO)_9$ is the source of the $Fe(CO)_3$ fragment, and $[Rh(CO)_2Cl]_2$ is the source of the $Rh(CO)_2$ fragment. The entering fragment is shown by the open circle with arrow, and its position in the product, by the circle with hash marks.

= *cis*-cyclooctene).[14] Thus, reaction 1 provides a good entry into the $[HFe_4(CO)_{12}HB]^-$ system. Unfortunately, reaction 1 appears to be unique to the hydrogen-rich triiron cluster $[HFe_3(CO)_9H_2BH]^-$. Application to other ferraborane monoanions gave either low yields of mixtures or no isolatable products whatsoever. Even worse, $[HFe_4(CO)_{12}HB]^-$ reacts but no new signals appear in the ^{11}B NMR spectrum and an intractable precipitate is the ultimate product.

However, another apparently unique reaction did produce a heterometal version of the desired boride. That is, the ferraborane anion $[HFe_4(CO)_{12}HB]^-$ or dianion $[Fe_4(CO)_{12}HB]^{2-}$ reacts cleanly and quantitatively with $[Rh(CO)_2Cl]_2$ to yield, via an uncharacterized intermediate, first 1,2-$[Rh_2Fe_4(CO)_{16}B]^-$ and then 1,6-$[Rh_2Fe_4(CO)_{16}B]^-$.[15,16] The final step, a cluster rearrangement, is conveniently slow but is promoted by the presence of uncoordinated soft bases.[17] Curiously, heterometal fragment sources used effectively by others in cluster-building reactions failed to provide similar routes to higher nuclearity products.

The extreme contrast between the two virtually quantitative cluster-binding reactions and all other attempts which failed was extremely puzzling. The known examples of boride clusters suggested no intrinsic instability of the high-nuclearity boride structure itself, suggesting that the origin of this bizarre behavior is mechanistic. Therefore, taking an optimistic view this system presented an opportunity to obtain information on cluster-building pathways. As the solution would also yield the desired homonuclear iron borides, we continued to pursue the problem, negative results notwithstanding. As it turns out, the key to the reaction lies in the one-electron properties of the reactant cluster relative to the iron carbonyl fragments serving as the cluster-building blocks. The cluster-building sequence described below, first empirically and then mechanistically, illustrates the process and provides a satisfying rationalization of the curious behavior of these ferraboranes.

Results and Discussion

Cluster-Building Reaction. The precursors for the $Fe(CO)_x$ fragments used to enlarge the $[Fe_4(CO)_{12}HB]^{2-}$ cluster were $Fe_2(CO)_9$ and $Fe(CO)_3(cco)_2$ (cco = *cis*-cyclooctene).[18] The important breakthrough took place when it was found that although $HFe_4(CO)_{12}H_2B$ and $[HFe_4(CO)_{12}HB]^-$ failed to produce any

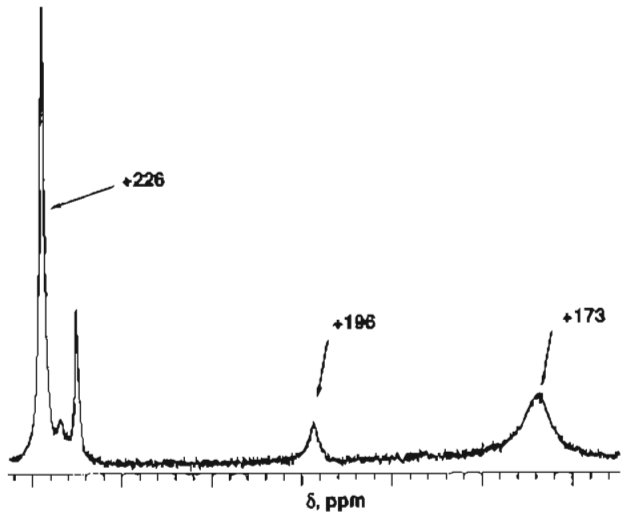

Figure 2. ^{11}B NMR spectrum of the products of the reaction of $[Fe_4(CO)_{12}HB]^{2-}$ with $Fe_2(CO)_9$ in THF at room temperature for 2 h. The mole ratio of ferraborane to $Fe_2(CO)_9$ = 0.17 (high stoichiometry reaction), 0.22 mmol of $[Fe_4(CO)_{12}HB]^{2-}$ was used, and the total yield of products (by NMR) was 80%.

useful products when reacted with either $Fe(CO)_x$ source under a variety of conditions, the reaction of the dianion, $[Fe_4(CO)_{12}HB]^{2-}$, gave a high total yield of isolatable products containing boron with a product distribution that depends on reaction stoichiometry.

^{11}B NMR was used to monitor the reaction, and Figure 2 illustrates the product spectrum for a typical reaction. The resonances at higher field were enhanced with shorter reaction times, high $[Fe_4(CO)_{12}HB]^{2-}$ to $Fe(CO)_x$ ratios, and the use of $Fe_2(CO)_9$ vs $Fe(CO)_3(cco)_2$ as the Fe fragment sources. That is, both fragment sources gave the same products but for the same mole ratio of dianion to iron fragment the $Fe(CO)_3(cco)_2$ source led to more of the higher nuclearity products. This is consistent with its higher reactivity. Based on the integration of the ^{11}B NMR signals relative to an external reference, the overall yield of products is ≈80%. Isolated yields of individual products, however, were ≈10%.

We have previously demonstrated an empirical correlation,[19] which was later theoretically justified,[20] between the number of direct Fe—B interactions in a ferraborane and the magnitude of the downfield chemical shift. Thus, the sequential buildup of products with increasingly downfield chemical shifts suggests that a cluster-building process is taking place. The downfield shifts were accompanied by decreasing line widths, showing loss of B—H interactions and an increasingly symmetrical environment for the boron atom. The products with the most positive chemical shifts had line widths characteristic of the highly symmetrical environment of an interstitial hole of a closed metal cluster.[15]

Finally, just as in reaction 1, the major byproduct of the reaction of $Fe_2(CO)_9$ with the dianion is $Fe(CO)_5$. This appears to be a characteristic feature of the cluster-building reaction. The reactions proceeded rapidly at room temperature even with the poorly soluble $Fe_2(CO)_9$ reagent. Although product distributions and total yields of ferraboranes were generally reproducible, actual yields of a given product under apparently similar conditions had large scatter.

No conditions permitted the formation of a single product, and we could not establish a stoichiometric equation similar to (1). Further, purification by fractional crystallization of these sensitive,

(14) Meng, X.; Bandyopadhyay, A. K.; Fehlner, T. P.; Grevels, F.-W. *J. Organomet. Chem.* **1990**, *394*, 15.
(15) Khattar, R.; Puga, J.; Fehlner, T. P.; Rheingold, A. L. *J. Am. Chem. Soc.* **1989**, *111*, 1877.
(16) Bandyopadhyay, A. K.; Khattar, R.; Puga, J.; Fehlner, T. P.; Rheingold, A. L. *Inorg. Chem.* **1992**, *31*, 465.
(17) Bandyopadhyay, A. K.; Khattar, R.; Fehlner, T. P. *Inorg. Chem.* **1989**, *28*, 4434.
(18) Fleckner, H.; Grevels, F.-W.; Hess, D. *J. Am. Chem. Soc.* **1984**, *106*, 2027.
(19) Rath, N. P.; Fehlner, T. P. *J. Am. Chem. Soc.* **1988**, *110*, 5345.
(20) Khattar, R.; Fehlner, T. P.; Czech, P. T. *New. J. Chem.* **1991**, *15*, 705.

Table 1. ^{11}B NMR Data for Metal–Boron Clusters

cluster	δ (ppm)[a]	fwhm (Hz)	fwhm {^1H} (Hz)	cation, solvent
$[Fe_4(CO)_{12}BH]^{2-}$	153 br s	280	240	PPN, THF
1,2-$[Rh_2Fe_4(CO)_{16}B]^-$	204.4 t J_{RhB} = 23.3 Hz	11	11	Li, THF
1,6-$[Rh_2Fe_4(CO)_{16}B]^-$	211.3 t J_{RhB} = 25.8 Hz	11	11	Li, THF
$[Fe_5(CO)_{15}BH]^{2-}$ (1)	173 br s	210	180	PPN, THF
$[HFe_6(CO)_{17}B]^{2-}$ (2)	196 br s	91	92	PPN, THF
$[HFe_7(CO)_{20}B]^{2-}$ (3)	226 d J_{BH} = 5 Hz[b]	19	15	PPN, Et_2O

[a] Relative to $\delta(BF_3{\cdot}Et_2O) = 0$. [b] Splitting independent of field strength.

Table 2. ^1H NMR Data for Metal–Boron Clusters[a]

cluster	δ (ppm)[b]	fwhm (Hz)	min T of variable temp (°C)
1	−11.2 br s	60	−55
2	no hydride obsd		
3	−20.6 s	30	−90

[a] $[AsPh]^+$ salts in THF-d_8, δ(Ph) = 7.6–7.5.

Table 3. Mass Spectrometric Data for Metal–Boron Clusters[a]

cluster	parent m/e	calcd m/e, compn	no. of CO losses	isotope pattern: p + 1, p, p − 1, p − 2
1	710.60	710.61, $C_{15}O_{15}Fe_5B$	11	obsd: 29, 100, 29, 32 calcd: 29, 100, 31, 31
2	822.47	822.53, $C_{17}O_{17}Fe_6B$	11	obsd: 33, 100, 32, 35 calcd: 31, 100, 33, 38
3	962.2	962.45, $C_{20}O_{20}Fe_7B$	17	obsd: 35, 100, 37, 40 calcd: 36, 100, 36, 44

[a] Negative FAB; NBA matrix; PPN salts.

Table 4. Infrared Data for Metal–Boron Clusters[a]

cluster	ν (cm^{-1}) (rel int)
1	1964 (s, sh), 1957 (vs), 1943 (s), 1893 (w, sh), 1745 (vw, br)
2	2012 (vs), 1990 (vs, br), 1964 (m), 1943 (m)
3	2081 (w), 1963 (vs), 1942 (s, sh), 1778 (w, br)

[a] Carbonyl region only; THF solvent; PPN cation.

but stable, dianions was unsuccessful. However, Dahl et al.[21] have described the successful separation of a similarly complex mixture of anionic clusters. We found that, by using his approach and by carrying out separations at low temperatures, we were able to isolate all three major products as pure compounds. These have been spectroscopically characterized and, in one case, crystallographically characterized. Some unstable intermediate compounds and minor products were observed by ^{11}B NMR; however, none were fully characterized, and consequently, their composition and structure remain unknown. The characteristics of each of the isolated compounds are described next.

Characterization of Products. The spectroscopic data are given in Tables 1–4, and compounds **1**–**3** are identified in Table 1 and Figure 3. As the characteristics of the ^{11}B NMR signal contain considerable useful information on this type of compound, the ^{11}B NMR data on the reactant, $[Fe_4(CO)_{12}HB]^{2-}$, and two octahedral boride anions are also given in Table 1 for comparative purposes.

$[HFe_5(CO)_{15}B]^{2-}$ (1). The major product formed at high $[Fe_4(CO)_{12}HB]^{2-}$ to $Fe(CO)_x$ ratios and short times has a ^{11}B chemical shift 20 ppm downfield from that of the reactant, suggesting one more Fe—B interaction, i.e., five direct Fe—B interactions. The line width is large and decreases on proton decoupling, demonstrating an asymmetrical boron environment and bonding to a hydrogen atom. The ^1H NMR evidences only one type of cluster hydrogen. The chemical shift and line width for the hydrogen show that it is involved in a B—H—Fe bridging interaction of some type.

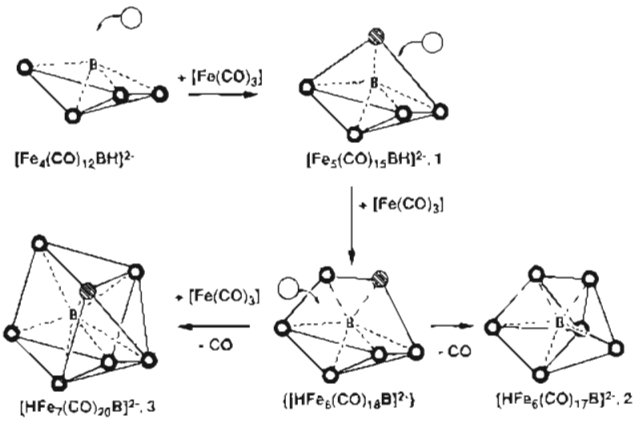

Figure 3. Schematic drawing of the cluster-building reaction beginning with $[Fe_4(CO)_{12}HB]^{2-}$. The open circle with arrow indicates the entering $Fe(CO)_x$ fragment, and the circle with hash marks in the products, the position it occupies in the boride.

The FAB MS exhibits the $[Fe_5(CO)_{15}B]^-$ ion which is only consistent with an even-electron cluster product composition and charge of $HFe_5(CO)_{15}B$, $\{Fe_5(CO)_{15}B\}^-$, or $[HFe_5(CO)_{15}B]^{2-}$. On the basis of solubility, the first is not possible, and on the basis of the coupling observed in the ^{11}B NMR plus the ^1H NMR resonance, the second is not possible either. Thus, we formulate the product as $[HFe_5(CO)_{15}B]^{2-}$ (**1**). It is interesting to note that fast atom bombardment of all the compounds reported here results in the "ionization" of the dianion by formal loss of H^- to give a monoanionic species of odd mass in the spectrometer.

The infrared spectrum is not particularly structurally informative, but the carbonyl band energies are consistent with the high-nuclearity dianion. That is, the shift to lower energy on deprotonation of a neutral metal carbonyl cluster decreases from $B_2H_6Fe_2(CO)_6$ to $HFe_3(CO)_9H_3BH$ to $HFe_4(CO)_{12}H_2B$. Therefore, the relatively high average energy of the CO stretching bands is still consistent with a dianion, provided the charge is either delocalized over a large number of metal carbonyl fragments or compensated by forming a tight ion pair with the cations. As the IR was not sensitive to cation, the former is more probable.

Apparent crystals of the compound (PPN and $AsPh_4$ derivatives) did not diffract. However, this ferraborane is an analog of $HOs_5(CO)_{16}B$, which has been described by Shore and mentioned above (Chart 1d). Hence, we postulate the structure shown in Figure 3, where neither the hydrogen nor carbonyl ligands are shown. As described by Shore et al., the structure is based on a pentagonal bipyramidal deltahedron in which two nonadjacent beltline vertices are vacant (Chart 2). Consequently, it is viewed as an arachno cluster and the electron count of 76 is consistent with the structure. Carbido analogs also exist.[22]

$[HFe_6(CO)_{17}B]^{2-}$ (2). A product observed at low $[Fe_4(CO)_{12}HB]^{2-}$ to $Fe(CO)_x$ ratios and longer times has a ^{11}B chemical shift 23 ppm downfield from that of **1**, suggesting six Fe—B interactions. It shows a smaller line width and no apparent coupling to protons. The magnitude of the line width suggests a still fairly asymmetrical boron environment and rules out a closed boride structure. The ^1H NMR shows resonances due to the cation but only very weak hydride resonances that can be accounted for by the presence of small amounts of the other products. However, this does not necessarily rule out the presence of a cluster hydride.

The FAB MS shows a $[Fe_6(CO)_{17}B]^-$ ion, which is consistent with either $HFe_6(CO)_{17}B$, $[Fe_6(CO)_{17}B]^-$, or $[HFe_6(CO)_{17}B]^{2-}$.

(21) Rieck, D. F.; Gavney, J. A., Jr.; Norman, R. L.; Hayashi, R. K.; Dahl, L. F. *J. Am. Chem. Soc.* **1992**, *114*, 10369.

(22) Mingos, D. M. P.; May, A. S. In *The Chemistry of Metal Cluster Complexes*; Shriver, D. F., Kaesz, H. D., Adams, R. D., Eds.; VCH: New York, 1990.

Chart 2

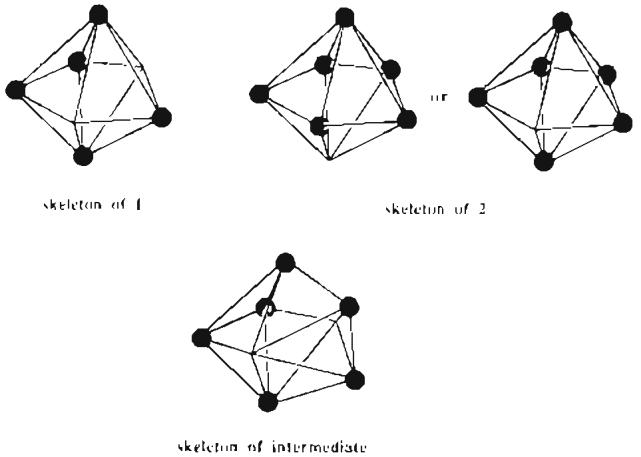

However, the solubility does not permit formulation as the neutral species. Again the IR is not too informative but supports a high-nuclearity boride anion.

Crystals of the $[AsPh_4]^+$ salt were obtained, and a data set was collected (monoclinic, space group $C2/c$, a = 22.007(4) Å, b = 10.550(2) Å, c = 25.579(4) Å, β = 100.01(2)°, Z = 4, V = 5848(4) Å^3). Two $[AsPh_4]^+$ ctaions were located and refined, providing unambiguous evidence for a dianion. Thus, the cluster is formulated as $[HFe_6(CO)_{17}B]^{2-}$.

Unfortunately, the dianionic iron cluster (>6 Fe) was severely disordered and no solution has been forthcoming. further, in this case we have no structural analogs with which to compare **2**. But the spectroscopic data and electron-counting rules provide a reasonable possibility. The line width of the ^{11}B resonance rules out a closed octahedral or prismatic structure, and these closed structures are also inconsistent with the electron count of **2**. However, the electron count of 88 is consistent with a nido structure, and thus, we postulate the structure shown in Figure 3. Like **1**, it is derived from a pentagonal bipyramidal deltahedron with one beltline vertex unoccupied (Chart 2). Of course, the other isomer derived by leaving an axial vertex vacant is also possible. One of the intermediates observed in the ^{11}B NMR (δ = 189, fwhm 120 Hz, $\{^1H\}$ 95 Hz) might be the arachno compound $[HFe_6(CO)_{18}B]^{2-}$, resulting directly from the addition of $Fe(CO)_3$ to **1**. This compound is a product in the reaction utilizing $Fe(CO)_3(cco)_2$ at low temperature, and it decomposes on warming. As it is only observed in a mixture, decomposition to **2** cannot be established; however, a reasonable structure based on the electron-counting rules is a dodecahedron with two vertices vacant (Chart 2). This could be easily formed from **1** as shown.

$[HFe_7(CO)_{20}B]^{2-}$ (3). The major product at low $[Fe_4(CO)_{12}HB]^{2-}$ to $Fe(CO)_x$ ratios or long times is compound **3**. It has a ^{11}B chemical shift which is yet another 30 ppm further downfield, suggesting seven Fe—B interactions. The line width is very narrow for boron and approaches that observed previously for the $[Rh_2Fe_4(CO)_{16}B]^-$ system. In the $[Rh_2Fe_4(CO)_{16}B]^-$ boride the boron atom relaxes relatively slowly due to the low asymmetry of its electronic environment. Thus, a highly symmetrical boron environment must exist in **3**. Further, the signal from **3** is a doublet (Figure 4) that collapses to a singlet on proton decoupling. The coupling constant is small enough to rule out a one-bond coupling which, because of the "relaxation curtain",[23] is ordinarily the only type of coupling observed for boron. In the ^1H NMR spectrum the proton is found in the FeHFe region showing that the B—H coupling is indeed a remote one. The NMR behavior is unambiguous in showing that this product is a closed metal boride; however, it gives no information on the geometric arrangement of the metal atoms.

(23) Kidd, R. G. In *NMR of Newly Accessible Nuclei*; Laszlo, P., Ed.; Academic Press: New York, 1983; Vol. 2; p 49.

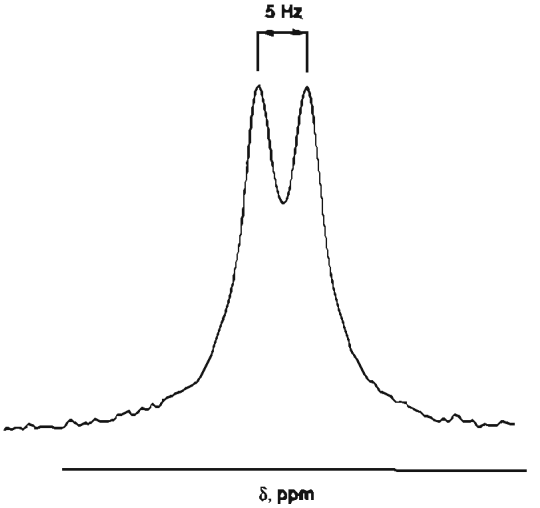

Figure 4. 160-MHz ^{11}B NMR spectrum of $[PPN]_2$ [3] in Et_2O showing the unusual n-bond coupling of the interstitial boron atom with an iron framework hydride.

Table 5. Crystal Data for $[Ph_4As]_2[3]$

chem formula	$[Ph_4As]_2[HFe_7B(CO)_{20}]$
fw	1729.66
cryst color	black
cryst size (mm^3)	0.39 × 0.19 × 0.11
space group	$P2_1/c$ (No. 14)
T (°C)	20 °C
a (Å)	11.248(2)
b (Å)	14.336(2)
c (Å)	41.698(6)
β (deg)	90.30(1)
V (Å^3)	6724(2)
Z	4
ρ_{calc} (g cm^{-3})	1.709
μ(Mo Kα) (cm^{-1})	25.153
R_1[a]	0.042 26
R_2[b]	0.056 93

[a] $R_1 = \Sigma||F_o| - |F_c||/\Sigma|F_o|$. [b] $R_2 = (\Sigma w(F_o - F_c)^2/\Sigma wF_o^2)^{1/2}$.

The FAB spectrum shows a $[Fe_7(CO)_{20}B]^-$ ion, which is consistent with either $HFe_7(CO)_{20}B$, $[Fe_7(CO)_{20}B]^-$, or $[HFe_7(CO)_{20}B]^{2-}$. Again solubility properties eliminate the first and the ^1H NMR data eliminate the second. Hence the complex is formulated as $[HFe_7(CO)_{20}B]^{2-}$. The IR data are consistent with the other spectroscopic information and suggest the presence of a bridging CO. Single crystals of the $[AsPh_4]^+$ derivative were obtained, and the structure solution (below) gave a composition $[AsPh_4]_2[HFe_7(CO)_{20}B]$, consistent with the FAB MS data.

Structure of 3. Crystal data and selected geometric parameters are given in Tables 5–7, and the ORTEP diagram of the dianion is shown in Figure 5. Six of the iron atoms are arranged in an approximately trigonal prismatic geometry and encapsulate a single bond atom. The seventh iron atom, Fe(5), with two terminal CO ligands caps a nearly square face with two Fe—Fe and two Fe—(μ-CO)—Fe interactions. Bridged interactions are shorter than unbridged (2.563(2) vs 2.635(2) Å), resulting in a slight fold along a line connecting Fe(1) and Fe(3). Both of these average distances are shorter than the Fe—Fe distances (average 2.74(3) Å) of the square face capped by Fe(5). The rest of the CO's are bound in terminal arrangements; however, the C(10)— and C(4)—metal distances suggest some semibridging character. The other two four-sided faces of the trigonal prism are rectangular, as expected.

The Fe—B distances for the six iron atoms making up the trigonal prism are within the normal range expected. However, the boron atom is not symmetrically located in the trigonal prism of iron atoms, being somewhat farther from Fe(6) and Fe(7) than the other four iron atoms (average 2.140(8) vs 2.034(8) Å). This, plus the shorter Fe—Fe distances joining Fe(5) to the prism,

Table 6. Final Atomic Coordinates and Equivalent Isotropic Thermal Parameters for **3**

atom	x	y	z	B_{eq} (Å^2)[a]	atom	x	y	z	B_{eq} (Å^2)[a]
Fe(1)	0.1434(1)	0.15662(8)	0.58149(3)	3.17(2)	C(21)	0.7710(6)	0.6093(5)	0.5575(2)	3.1(2)
Fe(2)	0.0148(1)	0.26066(8)	0.62402(3)	3.32(3)	C(22)	0.7104(7)	0.5907(6)	0.5290(2)	4.3(2)
Fe(3)	0.2236(1)	0.31703(8)	0.65198(3)	3.81(3)	C(23)	0.6538(8)	0.5044(7)	0.5266(2)	5.3(2)
Fe(4)	0.3515(1)	0.20530(8)	0.61123(3)	3.63(3)	C(24)	0.6597(7)	0.4411(6)	0.5508(2)	5.5(2)
Fe(5)	0.1934(1)	0.32905(8)	0.59124(3)	3.38(3)	C(25)	0.7186(7)	0.4596(6)	0.5784(2)	5.2(2)
Fe(6)	0.0652(1)	0.08576(8)	0.63716(3)	3.64(3)	C(26)	0.7749(7)	0.5455(6)	0.5820(2)	4.6(2)
Fe(7)	0.2707(1)	0.13903(9)	0.6618(3)	3.81(3)	C(27)	0.7434(7)	0.8244(5)	0.5515(2)	3.1(2)
C(1)	0.0276(7)	0.1111(6)	0.5578(2)	4.0(2)	C(28)	0.6285(8)	0.8174(6)	0.5623(2)	4.9(2)
O(1)	−0.0375(6)	0.0815(5)	0.5391(2)	6.6(2)	C(29)	0.5516(8)	0.8911(7)	0.5565(3)	6.7(3)
C(2)	0.2390(7)	0.0714(6)	0.5654(2)	4.1(2)	C(30)	0.5907(8)	0.9655(7)	0.5395(2)	5.8(3)
O(2)	0.2959(5)	0.0162(4)	0.5533(2)	5.8(2)	C(31)	0.7030(9)	0.9725(6)	0.5293(2)	5.5(2)
C(3)	0.1749(7)	0.2461(6)	0.5509(2)	3.8(2)	C(32)	0.7806(8)	0.8997(6)	0.5346(2)	4.5(2)
O(3)	0.1860(5)	0.2622(4)	0.5233(1)	4.7(2)	C(33)	0.9946(6)	0.7282(6)	0.5379(2)	3.2(2)
C(4)	−0.0697(8)	0.2162(7)	0.6565(2)	4.9(2)	C(34)	1.0722(7)	0.8015(6)	0.5430(2)	4.1(2)
O(4)	−0.1378(6)	0.2037(5)	0.6763(2)	7.7(2)	C(35)	1.1773(7)	0.8049(6)	0.5258(2)	4.6(2)
C(5)	−0.0327(7)	0.3764(6)	0.6311(2)	4.4(2)	C(36)	1.2009(8)	0.7367(7)	0.5034(2)	5.3(2)
O(5)	−0.0678(6)	0.4495(4)	0.6362(2)	6.4(2)	C(37)	1.1243(8)	0.6657(7)	0.4984(2)	5.4(2)
C(6)	−0.0970(8)	0.2453(6)	0.5938(2)	4.3(2)	C(38)	1.0183(7)	0.6603(6)	0.5157(2)	4.6(2)
O(6)	−0.1760(5)	0.2400(4)	0.5769(2)	5.7(2)	C(39)	0.9032(7)	0.7400(5)	0.6058(2)	2.9(2)
C(7)	0.3443(8)	0.3609(6)	0.6747(2)	5.4(2)	C(40)	0.8504(7)	0.8054(6)	0.6260(2)	4.0(2)
O(7)	0.4160(6)	0.3957(5)	0.6902(2)	8.8(2)	C(41)	0.8936(8)	0.8150(6)	0.6561(2)	4.7(2)
C(8)	0.1242(8)	0.3552(6)	0.6814(2)	4.9(2)	C(42)	0.9895(8)	0.7620(7)	0.6664(2)	5.5(2)
O(8)	0.0668(6)	0.3868(5)	0.7015(1)	6.7(2)	C(43)	1.0424(8)	0.6992(7)	0.6472(2)	5.7(3)
C(9)	0.2175(7)	0.4258(6)	0.6273(2)	4.2(2)	C(44)	0.9983(7)	0.6877(6)	0.6162(2)	4.4(2)
O(9)	0.2205(6)	0.5070(4)	0.6276(2)	5.8(2)	As(2)	0.50779(7)	0.70411(6)	0.68869(2)	3.20(2)
C(10)	0.4096(8)	0.0934(6)	0.6198(2)	4.6(2)	C(45)	0.3642(7)	0.6930(6)	0.7124(2)	3.5(2)
O(10)	0.4587(6)	0.0236(5)	0.6198(2)	7.2(2)	C(46)	0.3460(8)	0.7498(6)	0.7386(2)	5.0(2)
C(11)	0.4168(7)	0.2087(6)	0.5722(2)	4.5(2)	C(47)	0.241(1)	0.7398(7)	0.7556(2)	6.5(3)
O(11)	0.4648(6)	0.2103(5)	0.5480(1)	6.6(2)	C(48)	0.1587(8)	0.6756(7)	0.7457(2)	5.7(2)
C(12)	0.4717(9)	0.2755(8)	0.6254(2)	6.2(3)	C(49)	0.1788(8)	0.6179(7)	0.7205(2)	5.2(2)
O(12)	0.5550(6)	0.3165(6)	0.6325(2)	9.7(2)	C(50)	0.2820(7)	0.6270(6)	0.7032(2)	4.3(2)
C(13)	0.0879(7)	0.4039(6)	0.5734(2)	3.8(2)	C(51)	0.4627(6)	0.6883(5)	0.6451(2)	2.9(2)
O(13)	0.0273(6)	0.4553(4)	0.5601(2)	6.3(2)	C(52)	0.3760(8)	0.7445(6)	0.6327(2)	4.2(2)
C(14)	0.3093(7)	0.3850(6)	0.5707(2)	4.3(2)	C(53)	0.3356(8)	0.7298(6)	0.6011(2)	4.3(2)
O(14)	0.3765(6)	0.4236(5)	0.5552(2)	6.3(2)	C(54)	0.3834(7)	0.6585(7)	0.5833(2)	4.6(2)
C(15)	0.0298(8)	0.0382(6)	0.6751(2)	4.6(2)	C(55)	0.4689(7)	0.6010(6)	0.5966(2)	4.5(2)
O(15)	0.0051(6)	0.0041(5)	0.6992(1)	6.5(2)	C(56)	0.5092(7)	0.6153(6)	0.6268(2)	3.7(2)
C(16)	−0.0753(8)	0.0535(6)	0.6191(2)	4.4(2)	C(57)	0.5824(7)	0.8227(5)	0.6956(2)	3.4(2)
O(16)	−0.1648(6)	0.0310(5)	0.6102(2)	6.2(2)	C(58)	0.6450(9)	0.8351(7)	0.7241(2)	5.8(3)
C(17)	0.1355(8)	−0.0130(6)	0.6210(2)	4.5(2)	C(59)	0.7002(9)	0.9190(7)	0.7296(2)	6.3(3)
O(17)	0.1709(6)	−0.0822(4)	0.6117(2)	6.4(2)	C(60)	0.6964(8)	0.9864(7)	0.7068(2)	5.6(2)
C(18)	0.4099(8)	0.1675(6)	0.6845(2)	4.9(2)	C(61)	0.6375(8)	0.9746(6)	0.6788(2)	5.0(2)
O(18)	0.4955(6)	0.1820(5)	0.6979(2)	7.2(2)	C(62)	0.5802(7)	0.8902(6)	0.6727(2)	4.2(2)
C(19)	0.1906(7)	0.1732(6)	0.7012(2)	4.4(2)	C(63)	0.6198(7)	0.6123(6)	0.7028(2)	3.7(2)
O(19)	0.1448(6)	0.1871(5)	0.7248(1)	6.0(2)	C(64)	0.7316(8)	0.6103(7)	0.6900(2)	4.8(2)
C(20)	0.2826(8)	0.0170(6)	0.6744(2)	4.8(2)	C(65)	0.8151(8)	0.5500(7)	0.7008(2)	6.1(3)
O(20)	0.2946(6)	−0.0589(4)	0.6811(2)	5.8(2)	C(66)	0.788(1)	0.4940(8)	0.7261(3)	7.6(3)
B	0.1789(8)	0.2012(6)	0.6265(2)	2.7(2)	C(67)	0.676(1)	0.4957(6)	0.7403(2)	6.5(3)
As(1)	0.85169(7)	0.72532(6)	0.56231(2)	3.07(2)	C(68)	0.5894(8)	0.5559(6)	0.7286(2)	4.6(2)

[a] Isotropic equivalent displacement parameter defined as $(4/3)[a^2B(1,1) + b^2B(2,2) + c^2B(3,3) + ab(\cos\gamma)B(1,2) + ac(\cos\beta)B(1,3) + bc(\cos\alpha)B(2,3)]$.

results in a Fe(5)—B distance of 2.356(8) Å. Although long for a Fe—B bond, it is sufficiently short to justify a total of seven Fe—B interactions, as suggested by the ^{11}B NMR chemical shift. In a sense, the cluster is distorted such that Fe(5) and B can establish a bonding interaction.

The cluster hydrogen atom was not located. Considering that all phenyl hydrogens on the cations had electron densities around 1.0 e/Å^3 in a difference fourier map and that the highest residual peak in the final difference Fourier map had an electron density of only 0.56(9) e/Å^3, it is reasonable to assume that this hydrogen is disordered on several possible positions. The CO positions do not provide any compelling indication of where this hydrogen is located either.

The new boride **3** has a cluster electron count of 102, and its observed structure is consistent with the electron-counting rules. That is, a trigonal prismatic cluster requires 90 electrons and fusing a 74-electron square pyramidal M_5 cluster to one of its square faces permits a total count for the capped system of 102 or 100 for a count of 62 or 64 associated with the common shared square face, respectively.[24]

Although this is the first example of a boride structure possessing a square face capped trigonal prismatic structure, there are a few examples of carbide clusters with similar structures. One is $[Os_3Ni_4C(CO)_{15}]^{2-}$ (Chart 3).[25] In this cluster the carbide carbon atom is 0.7 Å farther away from the capping osmium atom than from the other two osmium atoms constituting part of the trigonal prism and is not considered to be bonded to it. This may be related to the heterometal nature of the cluster, as in $[Ni_7C(CO)_{12}]^{2-}$ (100 electrons) the carbide is bound to all seven nickel atoms.[26]

The electron count of the carbide analogs of **3** is 100. As noted already, this is still consistent with the electron-counting rules. The origin of this "flexibility" in electron count resides in the nature of the capping interaction. As presented by Mingos and Wales, a count of 62 for the common square face is associated with bonding analogous to that of $C_4H_4^{2-}$ whereas a count of 64 is associated with bonding analogous to that of a square planar transition metal cluster.[24] As the common square face in both

(24) Mingos, D. M. P.; Wales, D. J. *Introduction to Cluster Chemistry*; Prentice-Hall: New York, 1990.
(25) Karet, G. B.; Espe, R. L.; Stern, C. L.; Shriver, D. F. *Inorg. Chem.* **1992**, *31*, 2658.
(26) Ceriotti, A.; Piro, G.; Longoni, G.; Manassero, M.; Masciocchi, N.; Sansoni, M. *New. J. Chem.* **1988**, *12*, 501.

Table 7. Selected Bond Distances (Å) and Angles (deg) for **3**

Fe(1)—Fe(2)	2.736(2)[a]	Fe(3)—Fe(7)	2.672(2)	Fe(6)—Fe(7)	2.713(2)	C(6)—O(6)	1.13(1)
Fe(1)—Fe(4)	2.735(2)	Fe(3)—C(7)	1.768(9)	Fe(6)—C(4)	2.543(9)[b]	C(7)—O(7)	1.14(1)
Fe(1)—Fe(5)	2.567(2)	Fe(3)—C(8)	1.752(9)	Fe(6)—C(15)	1.771(9)	C(8)—O(8)	1.15(1)
Fe(1)—Fe(6)	2.686(2)	Fe(3)—C(9)	1.870(8)	Fe(6)—C(16)	1.807(9)	C(9)—O(9)	1.16(1)
Fe(1)—C(1)	1.756(8)	Fe(3)—B	2.033(8)	Fe(6)—C(17)	1.757(8)	C(10)—O(10)	1.14(1)
Fe(1)—C(2)	1.762(8)	Fe(4)—Fe(5)	2.644(2)	Fe(6)—B	2.140(9)	C(11)—O(11)	1.15(1)
Fe(1)—C(3)	1.844(8)	Fe(4)—Fe(7)	2.646(2)	Fe(7)—C(10)	2.575(8)[b]	C(12)—O(12)	1.14(11)
Fe(1)—B	2.021(8)	Fe(4)—C(10)	1.768(9)	Fe(7)—C(18)	1.786(9)	C(13)—O(13)	1.14(1)
Fe(2)—Fe(5)	2.626(2)	Fe(4)—C(12)	1.78(1)	Fe(7)—C(20)	1.788(9)	C(15)—O(15)	1.15(1)
Fe(2)—Fe(6)	2.628(2)	Fe(4)—B	2.048(9)	Fe(7)—B	2.140(8)	C(16)—O(16)	1.12(1)
Fe(2)—C(4)	1.777(9)	Fe(5)—C(3)	2.070(8)	C(1)—O(1)	1.15(1)	C(17)—O(17)	1.14(1)
Fe(2)—C(5)	1.768(9)	Fe(5)—C(9)	2.062(8)	C(2)—O(2)	1.14(1)	C(18)—O(18)	1.13(1)
Fe(2)—C(6)	1.790(9)	Fe(5)—C(13)	1.763(8)	C(3)—O(3)	1.183(9)	C(19)—O(19)	1.13(1)
Fe(2)—B	2.035(9)	Fe(5)—C(14)	1.756(8)	C(4)—O(4)	1.14(1)	C(20)—O(20)	1.13(1)
Fe(3)—Fe(4)	2.748(2)	Fe(5)—B	2.356(8)	C(5)—O(5)	1.14(1)		
Fe(3)—Fe(5)	2.560(2)						

Fe(2)—Fe(1)—Fe(4)	91.21(5)	Fe(1)—Fe(4)—Fe(3)	88.81(5)	C(15)—Fe(6)—C(16)	94.2(4)	Fe(4)—C(10)—O(10)	166.4(8)
Fe(2)—Fe(1)—Fe(5)	59.25(4)	Fe(1)—Fe(4)—Fe(5)	56.99(4)	C(15)—Fe(6)—C(17)	97.8(4)	Fe(7)—C(10)—O(10)	121.2(6)
Fe(2)—Fe(1)—Fe(6)	57.97(4)	Fe(1)—Fe(4)—Fe(7)	90.21(5)	C(15)—Fe(6)—B	128.4(4)	Fe(4)—C(11)—O(11)	176.2(8)
Fe(4)—Fe(1)—Fe(5)	59.72(4)	Fe(3)—Fe(4)—Fe(5)	56.65(4)	C(16)—Fe(6)—C(17)	91.7(4)	Fe(4)—C(12)—O(12)	173.9(9)
Fe(4)—Fe(1)—Fe(6)	89.32(5)	Fe(3)—Fe(4)—Fe(7)	59.36(4)	C(16)—Fe(6)—B	129.3(4)	Fe(5)—C(13)—O(13)	174.0(7)
Fe(5)—Fe(1)—Fe(6)	107.45(5)	Fe(5)—Fe(4)—Fe(7)	106.28(5)	C(17)—Fe(6)—B	105.8(4)	Fe(5)—C(14)—O(14)	173.3(7)
C(11)—Fe(1)—C(2)	88.9(4)	C(10)—Fe(4)—C(11)	93.2(4)	Fe(3)—Fe(7)—Fe(4)	62.21(4)	Fe(6)—C(15)—O(15)	177.1(8)
C(1)—Fe(1)—C(3)	90.8(4)	C(10)—Fe(4)—C(12)	99.6(4)	Fe(3)—Fe(7)—Fe(6)	90.15(5)	Fe(6)—C(16)—O(16)	174.7(8)
C(1)—Fe(1)—B	141.5(4)	C(10)—Fe(4)—B	105.1(4)	Fe(4)—Fe(7)—Fe(6)	90.62(5)	Fe(6)—C(17)—O(17)	172.8(8)
C(2)—Fe(1)—C(3)	95.6(4)	C(11)—Fe(4)—C(12)	88.3(4)	C(10)—Fe(7)—C(18)	81.1(3)	Fe(7)—C(18)—O(18)	175.2(8)
C(2)—Fe(1)—B	117.0(4)	C(11)—Fe(4)—B	132.7(4)	C(10)—Fe(7)—C(19)	172.9(3)	Fe(7)—C(19)—O(19)	173.0(8)
C(3)—Fe(1)—B	112.6(3)	C(12)—Fe(4)—B	129.2(4)	C(10)—Fe(7)—C(20)	81.4(4)	Fe(7)—C(20)—O(20)	175.8(8)
Fe(1)—Fe(2)—Fe(3)	88.96(5)	Fe(1)—Fe(5)—Fe(2)	63.58(4)	C(10)—Fe(7)—B	79.5(3)	Fe(1)—B—Fe(2)	84.8(3)
Fe(1)—Fe(2)—Fe(5)	57.17(4)	Fe(1)—Fe(5)—Fe(3)	96.88(5)	C(18)—Fe(7)—C(19)	91.9(4)	Fe(1)—B—Fe(3)	142.3(4)
Fe(1)—Fe(2)—Fe(6)	60.06(4)	Fe(1)—Fe(5)—Fe(4)	63.29(4)	C(18)—Fe(7)—C(20)	94.4(4)	Fe(1)—B—Fe(4)	84.5(3)
Fe(3)—Fe(2)—Fe(5)	56.95(4)	Fe(2)—Fe(5)—Fe(3)	63.75(5)	C(18)—Fe(7)—B	130.8(4)	Fe(1)—B—Fe(5)	71.4(2)
Fe(3)—Fe(2)—Fe(6)	90.53(5)	Fe(2)—Fe(5)—Fe(4)	95.77(5)	C(19)—Fe(7)—C(20)	98.6(4)	Fe(1)—B—Fe(6)	80.4(3)
Fe(5)—Fe(2)—Fe(6)	107.47(5)	Fe(3)—Fe(5)—Fe(4)	63.72(5)	C(19)—Fe(7)—B	105.9(4)	Fe(1)—B—Fe(7)	132.7(4)
C(4)—Fe(2)—C(5)	92.6(4)	C(3)—Fe(5)—C(9)	172.4(3)	C(20)—Fe(7)—B	126.2(4)	Fe(2)—B—Fe(3)	84.6(3)
C(4)—Fe(2)—C(6)	96.7(4)	C(3)—Fe(5)—C(13)	86.6(3)	Fe(1)—C(1)—O(1)	171.2(7)	Fe(2)—B—Fe(4)	146.4(4)
C(4)—Fe(2)—B	107.4(4)	C(3)—Fe(5)—C(14)	86.5(3)	Fe(1)—C(2)—O(2)	175.5(7)	Fe(2)—B—Fe(5)	73.0(3)
C(5)—Fe(2)—C(6)	91.3(4)	C(3)—Fe(5)—B	93.0(3)	Fe(1)—C(3)—Fe(5)	81.8(3)	Fe(2)—B—Fe(6)	78.0(3)
C(5)—Fe(2)—B	131.2(4)	C(9)—Fe(5)—C(13)	89.1(3)	Fe(1)—C(3)—O(3)	146.2(7)	Fe(2)—B—Fe(4)	84.6(3)
Fe(2)—Fe(3)—Fe(4)	90.88(5)	C(9)—Fe(5)—B	94.5(3)	Fe(2)—C(4)—Fe(6)	72.5(3)	Fe(3)—B—Fe(5)	70.9(3)
Fe(2)—Fe(3)—Fe(5)	59.30(4)	C(13)—Fe(5)—C(14)	90.9(4)	Fe(2)—C(4)—O(4)	165.9(8)	Fe(3)—B—Fe(6)	132.1(4)
Fe(2)—Fe(3)—Fe(7)	88.91(5)	C(13)—Fe(5)—B	133.5(3)	Fe(6)—C(4)—O(4)	121.1(7)	Fe(3)—B—Fe(7)	79.6(3)
Fe(4)—Fe(3)—Fe(5)	59.63(4)	C(14)—Fe(5)—B	135.5(3)	Fe(2)—C(5)—O(5)	177.1(8)	Fe(4)—B—Fe(5)	73.4(3)
Fe(4)—Fe(3)—Fe(7)	58.43(4)	Fe(1)—Fe(2)—Fe(2)	61.97(4)	Fe(2)—C(6)—O(6)	172.5(8)	Fe(4)—B—Fe(6)	131.0(4)
Fe(5)—Fe(3)—Fe(7)	107.98(5)	Fe(1)—Fe(6)—Fe(7)	89.82(5)	Fe(3)—C(7)—O(7)	173.9(8)	Fe(4)—B—Fe(7)	78.3(3)
C(7)—Fe(3)—C(8)	90.2(4)	Fe(2)—Fe(6)—Fe(7)	90.38(5)	Fe(3)—C(8)—O(8)	173.4(8)	Fe(5)—B—Fe(6)	140.8(4)
C(7)—Fe(3)—C(9)	91.4(4)	C(4)—Fe(6)—C(15)	82.1(4)	Fe(3)—C(9)—Fe(5)	81.1(3)	Fe(5)—B—Fe(7)	140.5(4)
C(7)—Fe(3)—B	139.3(4)	C(4)—Fe(6)—C(16)	78.4(3)	Fe(3)—C(9)—O(9)	145.7(7)	Fe(6)—B—Fe(7)	78.7(3)
C(8)—Fe(3)—C(9)	95.9(4)	C(4)—Fe(6)—C(17)	170.0(4)	Fe(5)—C(9)—O(9)	133.2(7)		
C(8)—Fe(3)—B	117.7(4)	C(4)—Fe(6)—B	81.7(3)	Fe(4)—C(10)—Fe(7)	72.4(3)		
C(9)—Fe(3)—B	112.6(3)						

[a] Numbers in parentheses are estimated standard deviations in the least significant digits. [b] Weak interaction.

boride and carbides is composed of four metal atoms, the difference in electron counts may reflect the differing metal properties.

It is significant that **3** corresponds very closely to the building block from which metal-rich, solid state metal borides are considered to be constructed.[27] This building block is shown in Chart 4. Depending on whether the face-capping atoms are metal or boron atoms, one can generate solid state borides with isolated B atoms, B_2 units, B_n chains, etc. by fusing such building blocks in an extended array. With face-capping positions 2 and 3 in Chart 4 vacant and with position 1 occupied by an iron atom, the core structure of **3** is reproduced. The trigonal prismatic boride core in Chart 4 is a much more common feature of solid state boride structures than is an octahedral arrangement.

Reaction Summary. Figure 3 summarizes the cluster-building process beginning with the four-iron cluster and ending with a seven-iron cluster. The three steps clearly involve the addition of an $Fe(CO)_3$ fragment and lead naturally to products that have precedent in the literature and obey the electron-counting rules.

(27) Greenwood, N. N.; Earnshaw, A. *Chemistry of the Elements*; Pergamon Press: Oxford, England, 1984.

2 is thought to arise from CO loss from the postulated arachno intermediate $[HFe_6(CO)_{18}B]^{2-}$. Other likely products are $[Fe_5(CO)_{14}BH]^{2-}$, analogous to $Fe_5(CO)_{15}C$, and $[HFe_6(CO)_{16}B^{2-}$, analogous to $HRu_6(CO)_{17}B$, which might be formed by CO loss from **1** and **2**, respectively.

Mechanism. A number of the observed features of this cluster-building process are highly suggestive of the nature of the reaction mechanism. The fact that the dianionic cluster reactant leads to high yields of products whereas the neutral and monoanionic cluster reactants do not suggest that either the dianion opens up a new pathway or the dianionic products are particularly stable vis á vis the neutral and monoanionic products. The set of fully characterized neutral and monoanionic borides does not support the latter postulate.

On the basis of (a) empirical stoichiometry of reaction 1, (b) the observation of $Fe(CO)_5$ as the principal iron byproduct in reaction 1, (c) the easy generation of iron carbonyl hydride radicals and the characterization of all non-boron radical intermediates thought important,[28,29] and (d) existing evidence for radical pathways in organometallic and cluster chemistries,[1,30] we

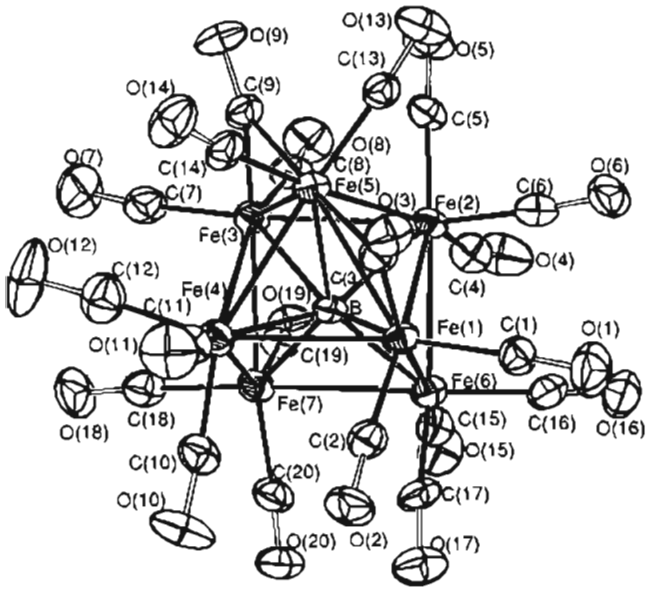

Figure 5. Structure of $[HFe_7(CO)_{20}B]^{2-}$ (**3**) in the $[AsPh_4]$ salt showing 40% probability ellipsoids and the atom-labeling scheme. The hydride is not shown.

Chart 3

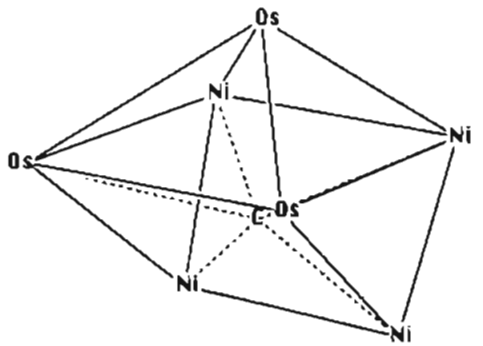

$[Os_3Ni_4C(CO)_{15}]^{2-}$

previously suggested the following mechanism for reaction 1:[31]

$$[HFe_3(CO)_9BH_3]^- + Fe_2(CO)_9 \rightarrow [Fe_3(CO)_9BH_3^{\bullet}]^- + HFe(CO)_4^{\bullet} + Fe(CO)_5 \quad (1a)$$

$$HFe(CO)_4^{\bullet} + Fe_2(CO)_9 \rightarrow HFe_2(CO)_8^{\bullet} + Fe(CO)_5 \quad (1b)$$

$$[Fe_3(CO)_9BH_3^{\bullet}] + HFe_2(CO)_8^{\bullet} \rightarrow [HFe_4(CO)_{12}BH]^- + H_2 + Fe(CO)_5 \quad (1c)$$

$$\text{net: } [HFe_3(CO)_9BH_3]^- + 2Fe_2(CO)_9 \rightarrow [HFe_4(CO)_{12}BH]^- + H_2 + 3Fe(CO)_5 \quad (1)$$

We viewed hydrogen atom transfer as the initial step and the loss of H_2 from this "hydrogen-rich" system as an important driving force. $HFe_2(CO)_8^{\bullet}$ is the effective source of the $Fe(CO)_3^{\bullet}$ radical building block. An analogous mechanism for the production of **1** can be written if it is postulated that electron transfer rather than hydrogen atom transfer initiates the process. This is shown in reaction 2, where now $[Fe_2(CO)_8^{\bullet}]^-$ is the effective source of

Chart 4

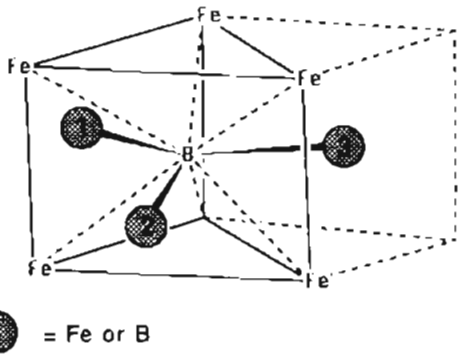

= Fe or B

$$[Fe_4(CO)_{12}BH]^{2-} + Fe_2(CO)_9 \rightarrow [Fe_4(CO)_{12}BH^{\bullet}]^- + [Fe(CO)_4^{\bullet}]^- + Fe(CO)_5 \quad (2a)$$

$$[Fe(CO)_4^{\bullet}]^- + Fe_2(CO)_9 \rightarrow [Fe_2(CO)_8^{\bullet}]^- + Fe(CO)_5 \quad (2b)$$

$$[Fe_4(CO)_{12}BH^{\bullet}]^- + [Fe_2(CO)_8^{\bullet}]^- \rightarrow [HFe_5(CO)_{15}B]^{2-} + Fe(CO)_5 \quad (2c)$$

$$\text{net: } [Fe_4(CO)_{12}BH]^{2-} + 2Fe_2(CO)_9 \rightarrow [HFe_5(CO)_{15}B]^{2-} + 3Fe(CO)_5 \quad (2)$$

the $[Fe(CO)_3^{\bullet}]^-$ radical anion building block. Again $Fe(CO)_5$ is the byproduct with $Fe_2(CO)_9$ as the cluster-building reagent.

Why should the dianion support (2) and not the monoanion? We do know that the Brönsted acidity of the neutral clusters increases substantially as the number of metal atoms in the cluster increases. As an extreme example, note that protonation of 1,6-$\{Rh_2Fe_4(CO)_{16}B]^-$ is accomplished only with difficulty.[16] Therefore, we suggest that the monoanion is both too poor a hydrogen atom and electron donor to initiate pathway 1 or 2. The dianion is a much better electron donor than the monoanion and can initiate electron transfer as indicated in (2). The fact that the hydrogen atom transfer process shuts down after the four-iron product is formed allows quantitative yields of $[HFe_4(CO)_{12}HB]^-$ to be isolated from reaction 1. As one expects the electron donor ability to decrease with increasing cluster size, the cluster-building efficiency should decrease accordingly. Thus for each cluster, **1**, **2**, or **3**, the formation reaction is faster than the depletion reaction, permitting significant amounts of each to be generated at the appropriate stoichiometry.

Thus, reaction 3 is suggested as the general mechanism for the cluster-building process observed here for $Fe_2(CO)_9$. Presumably

$$[HFe_x(CO)_yB]^{2-} + Fe_2(CO)_9 \rightarrow [HFe_x(CO)_yB^{\bullet}]^- + [Fe(CO)_4^{\bullet}]^- + Fe(CO)_5 \quad (3a)$$

$$[Fe(CO)_4^{\bullet}]^- + Fe_2(CO)_9 \rightarrow [Fe_2(CO)_8^{\bullet}]^- + Fe(CO)_5 \quad (3b)$$

$$[HFe_x(CO)_yB^{\bullet}]^- + [Fe_2(CO)_8^{\bullet}]^- \rightarrow [HFe_{x+1}(CO)_{12+3}B]^{2-} + Fe(CO)_5 \quad (3c)$$

$$\text{net: } [HFe_x(CO)_yB]^{2-} + 2Fe_2(CO)_9 \rightarrow [HFe_{x+1}(CO)_{12+3}B]^{2-} + 3Fe(CO)_5 \quad (3)$$

the reaction with $Fe(CO)_3(cco)_2$ is related. Although the proposed mechanism is speculative, as it is unsupported by direct evidence

(28) Fehlner, T. P. *New. J. Chem.* **1988**, *12*, 307.
(29) Krusic, P. J.; Filippo, J. S., Jr.; Hutchinson, B.; Hance, R. L.; Daniels, L. M. *J. Am. Chem. Soc.* **1981**, *103*, 2129.
(30) Krusic, P. J. *J. Am. Chem. Soc.* **1981**, *103*, 2131.
(31) Horwitz, C.P.; Holt, E. M.; Shriver, D. F. *Organometallics* **1985**, *4*, 1117.

such as kinetic studies, the body of circumstantial evidence is sufficiently compelling that the postulate is justified. At minimum, it provides an internally consistent description and suggests future approaches to the cluster-building problem.

Experimental Section

General Procedures. All manipulations were carried out under an atmosphere of argon or in a standard vacuum line using Schlenk techniques. Analytical grade solvents and deuterated solvents were properly dried, degassed, and freshly distilled before use. Spectra were recorded on the following instruments: IR, Nicolet 205 FTIR, using a 0.2-mm cell provided with a NaCl window: ^{1}H NMR, Varian 500-MHz or GN 300-MHz spectrometer, using residual solvent as reference; ^{11}B NMR, Nicolet 300-MHz spectrometer operating at 96 MHz, using $B_3H_8NMe_4$ (δ = –29.7 ppm) in acetone-d_6 as internal reference; FAB MS, JEOL JMS-AX505HA spectrometer with an NBA matrix. The following reagents were used as received without further purification, unless otherwise mentioned: $Fe_2(CO)_9$ (Aldrich), BH_3·THF (1.0 M in THF) (Aldrich), *n*-butyllithium (1.6 M in hexane) (Aldrich), HBF_4 (Strem). $AsPh_4Cl$ (Aldrich) and $(PPh_3)_2NCl$ (Aldrich) were dried at 55–60 °C for 3 days before use. $HFe_4(CO)_{12}BH_2$[13] and $Fe(CO)_3(cco)_2$ (cco = *cis*-cyclooctene)[18] were prepared by literature procedures. $HFe_4(CO)_{12}BH_2$ was deprotonated with 2 equiv of BuLi to form $Li_2Fe_4(CO)_{12}HB$.[32] Products were separated by column chromatography at variable temperature (+20 to –30 °C) by employing 60–200-mesh silica gel (Baker Analyzed) predried in oven at least for overnight and degassed for 3–4 h immediately before use. On occasion, further purification was achieved by fractional crystallization from a THF–hexane solvent mixture at –45 °C.

Reaction of $Fe(CO)_3(cco)_2$ with $[Fe_4(CO)_{12}HB]^{2-}$. A freshly prepared solution of $[Fe_4(CO)_{12}HB]^{2-}$, obtained by deprotonating 132 mg (0.23 mmol) of $HFe_4(CO)_{12}H_2B$ in 8 mL of THF with BuLi at –78 °C, was transferred to a Schlenk tube containing 515 mg (1.43 mmol) of $Fe(CO)_3(cco)_2$ (low-stoichiometry reaction) or 800 mg (2.22 mmol) of $Fe(CO)_3(cco)_2$ (high-stoichiometry reaction). The suspension was stirred for 1–2 h at –78 °C and allowed to stand overnight at –45 °C. The reaction mixture was then added to a solution of 140 mg (0.25 mmol) of PPNCl dissolved in 8 mL of THF. The reaction mixture was stirred for 1 h at room temperature. Solvent and volatiles were removed under reduced pressure. The residue was extracted with 10 mL of THF, and the extract was subjected to column chromatography (*vide infra*).

Reaction of $Fe_2(CO)_9$ with $[Fe_4(CO)_{12}HB]^{2-}$. A 6.0-mL THF solution of $[Fe_4(CO)_{12}HB]^{2-}$, freshly prepared from 120 mg (0.21 mmol) of $HFe_4(CO)_{12}H_2B$ with BuLi at –78 °C, was transferred to a Schlenk tube containing 148 mg (0.41 mmol) (low-stoichiometry reaction) or 470 mg (1.29 mmol) (high-stoichiometry reaction) of finely powdered $Fe_2(CO)_9$. The mixture was slowly warmed from –20 °C to ambient temperature over a period of ca. 2 h along with stirring. The stirring was continued at room temperature for an additional period of 3–4 h in the dark, during which time the diiron nonacarbonyl dissolved completely and the color of the resulting solution turned from dark brown to dark cherry-red. To this was added a solution of 125 mg (0.22 mmol) of (PPN)Cl or 126 mg (0.30 mmol) of $AsPh_4Cl$ dissolved in 5.0 mL of THF, and the mixture was stirred for 1 h at room temperature, after which the solvent and volatiles were removed under reduced pressure; the residue was washed successively with 150–20-mL portions of toluene up to a total volume of ca. 250 mL in order to separate the neutral products from the anions. Toluene extraction also permits removal of any non-boron metal cluster impurities.

Separation. For the low-stoichiometry reaction THF extract of the product mixture was loaded on a 2.5 cm × 15 cm silica gel column bed surrounded by a cold jacket containing an acetone–dry ice mixture at –20 °C. Elution with Et_2O containing 30% THF removed $[HFe_4(CO)_{12}HB]^-$ and $[Fe_4(CO)_{12}HB]^{2-}$ along with any non-boron compounds. The next fraction, collected by eluting with a solvent mixture of Et_2O and 70% THF, afforded **1** as a dark marroon solution in THF which is stable at room temperature but sensitive to water and oxygen. Dark maroon hexagonal flakes are formed on diffusion of hexanes into the THF solution (≈30 mg of the $AsPh_4$ salt, 10%). Spectroscopic properties are given in Tables 1–4.

For the high-stoichiometry reaction, the reaction mixture was first extracted with toluene. The concentrated toluene extract was treated on a silica gel column (1.5 cm × 16 cm) containing acidified silica gel (acidified with HBF_4, washed with water to remove free acid, dried in the oven, and degassed before use as usual). The column was washed with toluene to remove $HFe_4(CO)_{12}H_2B$ and any non-boron compounds. This was followed by a maroon-red fraction, collected by eluting with toluene containing 15% Et_2O, which afforded ≈35 mg of the $AsPh_4$ salt (10%) of **2**. This product is soluble in toluene, Et_2O, THF, and methanol, giving rise to maroon-red solutions which are stable at room temperature. Spectroscopic properties are given in Tables 1–4.

The residue after the toluene extraction was dissolved in 15 mL of a 1:1 mixture of Et_2O and THF and loaded on a column (2.5 cm × 10 cm). Elution with the same solvent mixture led to the removal of the residual portion of **2**. This was followed by elution with THF containing 10% methanol, which resulted in the separation of **1** as a mixture. This was purified by successive columns and finally by washing with toluene. A continued elution with the same solvent mixture led to the isolation of a dark violet compound (≈42 mg of the $AsPh_4$ salt of **3**, 12%). In case of $AsPh_4$ salts, **3** was eluted as a mixture of two compounds from which $[AsPh_4]_2$ [**3**] was extracted with methanol. This product is soluble in THF and CH_2Cl_2, somewhat soluble in methanol, and insoluble in Et_2O. Spectroscopic properties are given in Tables 1–4.

X-ray Structure Determination of 3. X-ray-quality crystals of $[AsPh_4]_2$ [**3**] were grown by slow diffusion of hexane into a THF solution layer in constricted glass tubing (5–8 mm) at low temperature (–5 to –14 °C). Preliminary examination and data collection were performed with Mo Kα radiation (λ = 0.710 73 Å) on an Enraf-Nonius CAD4 diffactometer equipped with a graphite-crystal, incident-beam monochromator. The crystallographic data are summarized in Table 5. Cell constants and an orientation matrix for data collection were obtained from least-squares refinement, using the setting angles of 25 reflections in the range $28° < 2\theta < 30°$. Data were collected using the ω-scan technique up to a 2θ of 46.0°. Full details are given in the supplementary material. At total of 9455 reflections were collected, of which 7827 were unique and not systematically absent and 5537, having intensities with $F_o^2 > 3\sigma(F_o^2)$, were taken as observed. Lorentz and polarization corrections were applied to the data. An empirical absorption correction based on a series of ψ scans was applied to the data. The structure was solved by direct methods and difference Fourier syntheses. The structure was refined by full-matrix least-squares techniques using anisotropic thermal parameters for non-hydrogen atoms. Phenyl hydrogen atoms were located and added to the structure factor calculations with their isotropic thermal parameters fixed at 1.1 times the B_{eq}'s of their bonded carbon atoms. Scattering factors were taken from Cromer and Waber.[33] The highest peak in the final difference Fourier map had a height of 0.56(9) e/Å^3, and the minimum negative peak had a height of –0.48(9) e/Å^3. The first several peaks were around metal atoms: lying along a metal–metal edge or capping a trigonal metal face. However, none of these peaks could be refined successfully as the hydride atom. Atom coordinates are given in Table 6, and selected bond distances, and angles, in Table 7.

Acknowledgment. The support of the National Science Foundation is gratefully acknowledged.

Supplementary Material Available: Text giving a full description of the structure determination, tables of experimental details, general displacement parameter expressions, positional and isotropic thermal parameters of hydrogen atoms, additional bond distances and bond angles, and least-squares planes, and drawings of the two $[AsPh_4]^+$ counterions for **3** (33 pages). Ordering information is given on any current masthead page.

(32) Rath, N. P.; Fehlner, T. P. *J. Am. Chem. Soc.* **1987**, *109*, 5273.

(33) Cromer, D. T.; Waber, J. T. *International Tables for X-ray Crystallography*; Kynoch Press: Birmingham, England, 1974; Vol. IV, Table 2.2B.